XA0202091

ION CHANNELING STUDY OF DEFECTS IN MULTICOMPONENT SEMICONDUCTOR COMPOUNDS

A. TUROS, L. NOWICKI, A. STONERT
The Andrzej Soltan Institute for Nuclear Studies,
Warsaw, Poland

Abstract

Compound semiconductor crystals are of great technological importance as basic materials for production of modern opto- and microelectronic devices. Ion implantation is one of the principal techniques for heterostructures processing. This paper reports the results of the study of defect formation and transformation in binary and ternary semiconductor compounds subjected to ion implantation with ions of different mass and energy. The principal analytical technique was He-ion channeling. The following materials were studied:, GaN and InGaN epitaxial layers. First the semi empirical method of channeling spectra analysis for ion implanted multicomponent single crystal was developed. This method was later complemented by the more sophisticated method based on the Monte Carlo simulation of channeling spectra. Next, the damage buildup in different crystals and epitaxial layers as a function of the implantation dose was studied for N, Mg, Te, and Kr ions. The influence of the substrate temperature on the defect transformations was studied for GaN epitaxial layers implanted with Mg ions. Special attention was devoted to the study of growth conditions of InGaN/GaN/sapphire heterostructures, which are important component of the future blue laser diodes. In-atom segregation and tetragonal distortion of the epitaxial layer were observed and characterized. Next problem studied was the incorporation of hydrogen atoms in GaAs and GaN. Elastic recoil detection (ERDA) and nuclear reaction analysis (NRA) were applied for the purpose.

1. Radiation Damage in InGaAs/InP Heterostructures

1.1. Background

InGaAs/InP epitaxial layers are of a great a great importance for optoelectronic applications, especially for development of high efficiency laser diodes. The energy gap of multicomponent semiconductors depends on the lattice constant, which according to the Vegard's law changes linearly with the content of a given component. The RBS technique is well suited for analysis surface layer composition. Furthermore, ion channeling is a well-established technique for determination of crystalline perfection. Thus, the reported experiments were carried out by means of the RBS/channeling technique. The 2 MeV ^{4}He beam from the Van de Graaff accelerator LECH at the Andrzej Sołtan Institute for Nuclear Studies was used.

1.2. Results

Fig. 1 shows the RBS random spectrum for the 1μm thick InGaAs/InP heterostructure. Such spectra can be evaluated using the RUMP code [1], which enables the calculation of the component spectra (also shown in Fig. 1). The relative height of each component spectrum is a measure of the content of corresponding element.

Fig. 2 shows the <100> aligned spectra for InGaAs epilayer before and after ion implantation with different doses of 100 keV Kr ions. The crystalline perfection of the investigated epilayer was determined by the comparison of the aligned spectrum with the random one. The typically obtained χ_{min} value of 4–5% indicated good quality of the virgin crystal.

Evaluation of channeling data measured for multicomponent samples requires special procedures. In the course of this project a graphic method of separation of channeling spectra from two different sublattices has been developed. In such a way one obtains two separate channeling spectra, which can be analyzed by means of the two-beam approximation [2].

Fig.3. shows the evolution of the defect depth distributions for different Kr-ion doses calculated using the described above method for GaAs sublattice. The defect distributions calculated with the TRIM code [3] are also shown for comparison.

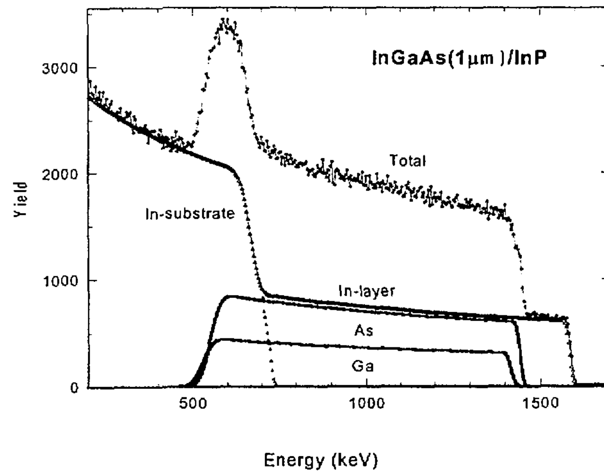

Fig. 1. RBS random spectrum for InGaAs(1μm)/InP heterostructure.

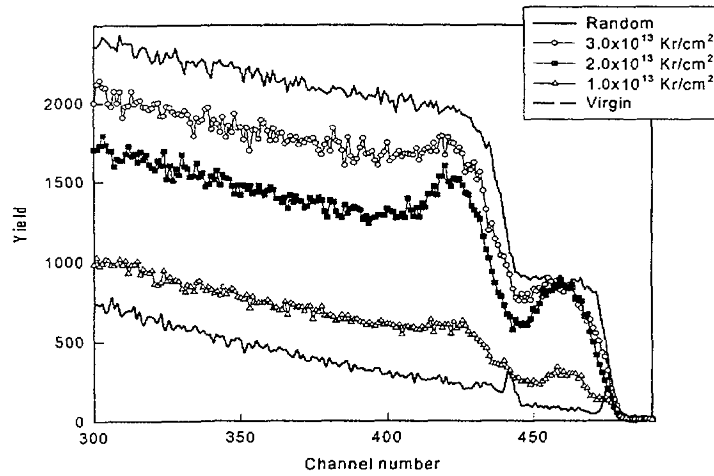

Fig. 2. Random and aligned spectra for InGaAs epilayer before and after ion implantation with different doses of 100 keV Kr ions.

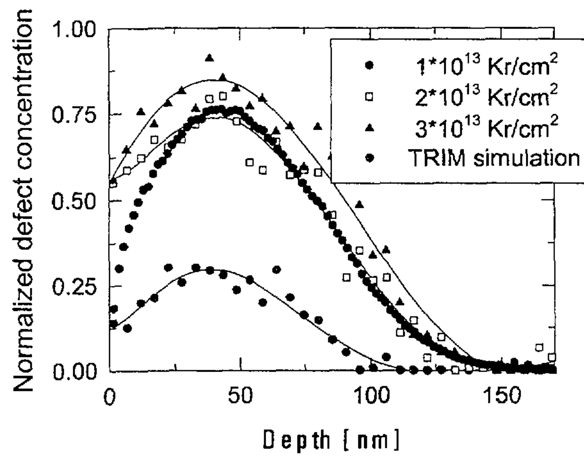

Fig. 3. Defect depth distributions in the GaAs sublattice produced by implantation with different Kr-ion doses.

The depth range of damage remains essentially the same for all indicated doses, however, the defect content increases at the beginning rapidly and shows the saturation effects at the dose of 3×10^{13} Kr/cm^2. It should be pointed out that the damage evolution in both sublattices is the same within the experimental error.

As illustrated in Fig. 4 for doses exceeding at 5×10^{13} As/cm^2 implanted regions became amorphous. With increasing ion dose the amorphous region extends to the greater depths, which is due to the accumulation of damage in the tail region of depth distributions of implanted ions.

InGaAs epilayers were also implanted with different doses of 100 keV N ions. In contrast to the heavy ion bombardment N-ion implantation did not produce important damage up to the dose of 5×10^{15} N/cm^2, i.e. ten times higher than the amorphisation dose for As-ion implantation. The maximum defect content was below 10 at.%. Since the higher doses are technologically irrelevant this experiment was stopped at this stage.

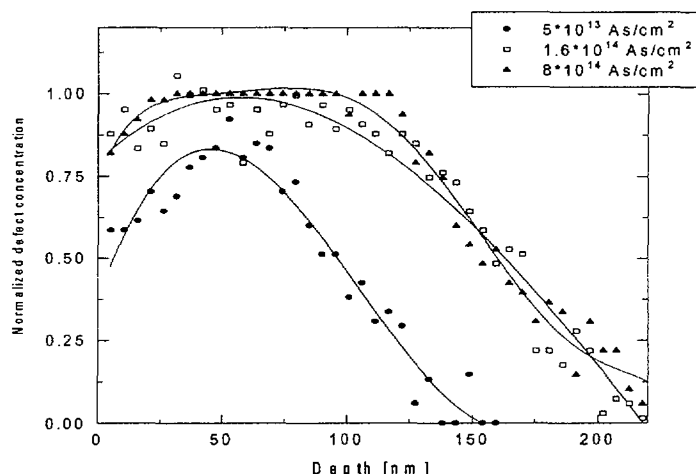

Fig. 4. Defect depth distributions in the GaAs sublattice produced by implantation with different As-ion doses.

1.3. Conclusions

The outcome of this part of the study can be summarized as follows:

- RBS/channeling is a suitable technique for the analysis of multicomponent epitaxial layers,
- InGaAs epitaxial layers of good crystalline quality can be produced by the metalorganic vapor deposition (MOCVD) technique,
- The procedure of spectra evaluation has been developed enabling the separate analysis of different sublattices of a layer,
- Both sublattices of InGaAs epitaxial layers exhibit the same damage buildup behavior upon ion implantation,
- The amorphisation dose at RT for 100 keV ions of mass about 80 amu amounts to 5×10^{13} at/cm^2,
- N-ion implantation produces only few defects in InGaAs, which is apparently due to the fact that according to the TRIM code calculations 100 keV N ions do not create collisions cascades.

2. Low Temperature Irradiation of GaN

2.1. Defect Mobility at Low Temperatures

Properties of defects in III-N semiconductor compounds have been extensively studied by various techniques over the last few years [4–8]. Point defects and their complexes determine the electrical properties of semiconductors, diffusion of impurities and the recovery of crystalline lattice after ion bombardment and subsequent annealing. Interstitial defects can be directly observed by the

RBS/channeling technique. As channeling is almost exclusively sensitive to displaced atoms, it has been expected that the application of this technique will provide valuable and complementary information on the defect structures in III-N compounds.

Ion implantation at 51 K with 150 keV N ions to fluences ranging from 0.5×10^{14}at/cm^2 to 6×10^{14}at/cm^2 and RBS/channeling measurements using 1.4 MeV He ions were carried out. The beams from an ion implanter and a Tandetron accelerator can be delivered to the same experimental chamber, which makes it possible to perform both ion implantation and RBS/channeling analysis without changing the temperature and the vacuum.

The experiment was performed in three stages: (i) the sample was mounted in a cryogenic goniometer and cooled down to 51 K where it was aligned and subsequently implanted with N ions, (ii) <0001> aligned channeling spectra were measured without changing the temperature at different time intervals, (iii) the sample was slowly warmed up to room temperature. During the warming-up, the aligned spectra were measured; the measurements time was about 10 min, and the corresponding temperature change was smaller than 4 K.

As can be seen in Fig. 5 the value of χ_{min}= 2% for the virgin crystal indicated its good crystalline perfection. The energy spectrum for the implanted sample exhibits continuous increase of the backscattering yield with implanted dose. Next the sample was warmed up to the room temperature. Only a small decrease of the channeling yield in the channel interval 140–200 can be noticed at 70 K. This is apparently due to the mobility of simple defects in the Ga sublattice. There are essentially no changes in the shape of the spectra up the temperature of 300 K.

2.2. Heavy Ion Bombardment

GaN single crystals were implanted with 150 keV Xe ions at 15 K to the fluence of 4.5×10^{14}Xe/cm^2. Fig. 6 shows the results of Xe-ion implantation. No changes in the damage peak (channels 360–400) were observed, whereas the low energy part of the spectrum continuously increased with increasing temperature. The constant area of the damage peak indicates that there are no defect transformations in the implanted region. The increase of dechanneling is attributed to the accumulation of defects produced by the analyzing beam.

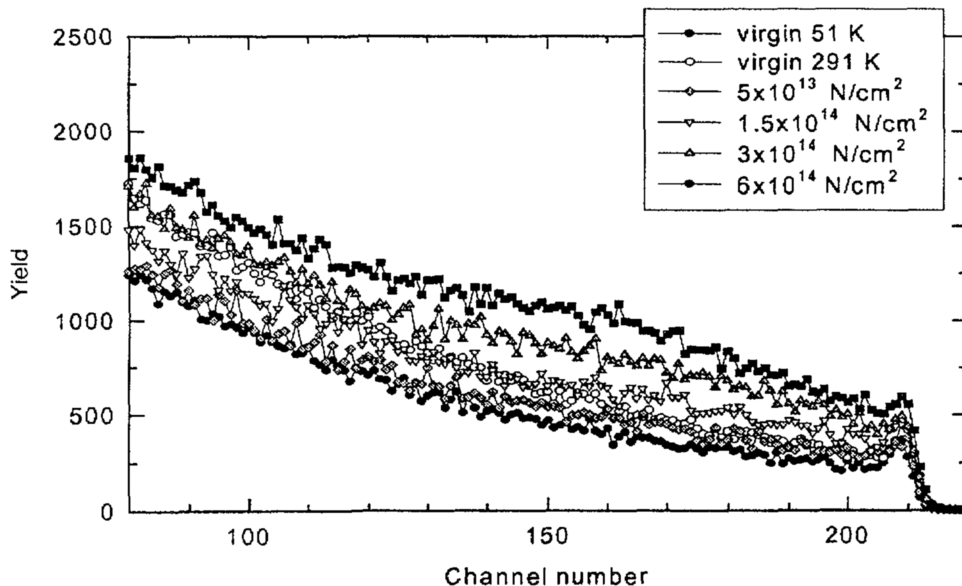

Fig. 5. <0001> aligned spectra for GaN single crystal before and after ion implantation with different doses of 150 keV N ions at 51 K.

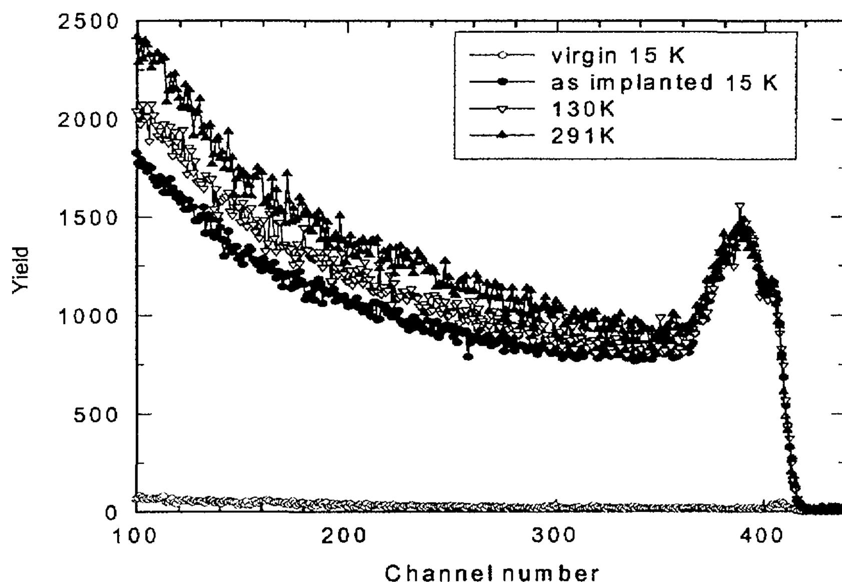

Fig. 6. The evolution of the spectra upon warming up to RT for GaN single crystal implanted with 4.5 × 10^{14} Xe/cm^2 at 15 K.

Similar experiment was performed for GaN sample implanted with Te ions. The evolution of the spectra upon warming up to RT reveals only a small decrease of the damage peak at 70 K. The minimum was attained at 130 K and is apparently due to the simple defect mobility. Their further clustering leads to the subsequent increase of the damage peak.

2.3. *Conclusions*

Small recovery stage in N ion implanted GaN observed at 70 K reveals the mobility of simple defect i.e., selfinterstitials or vacancies belonging to the Ga sublattice. The fact that the major part of defects is stable up to RT can be attributed to important defect clustering occurring even at very low temperatures. It is well know that implanted noble gas atoms are very effective in trapping defects, especially vacancies. The stability of defects in Xe-ion bombarded GaN can also be due to defect clustering around Xe atoms. In contrast, such an effect has not been observed in GaN implanted with miscible elements like Te.

3. Ion Implantation in GaN at High Temperatures

3.1. *Mg-ion Implantation*

GaN epitaxial layers on sapphire were implanted with Mg-ions at three different energies and doses (30 keV-2.8 × 10^{14} Mg/cm^2, 80 keV-7.0 × 10^{14} Mg/cm^2, and 200 keV-8 × 10^{14} Mg/cm^2) in order to obtain uniform depth distributions of dopants and defects extending from the surface up to the depth of approx. 300 nm. Ion implantation was performed at RT, 600°C, 700°C, and 800°C. The aim of this study was to introduce the p-dopants into the GaN crystals in a manner that might ensure their high electrical activity. Since ion bombardment induced defects in GaN are very resistant to annealing it was thought that ion implantation at high temperatures can facilitate both crystal lattice recovery and lattice site incorporation of dopant atoms. The structure of as-grown and implanted epilayers was examined using the RBS/channeling. Fig. 7 shows the aligned spectra for GaN epilayers implanted at different temperatures.

The ion implantation at RT produces a clearly visible damage peak between channels 600 and 700. One notes strong decrease of damage peak and the dechanneling behind it after implantation at 800°C. In order to elucidate the residual defect structure the energy dependent dechanneling analysis was performed. Such measurements are based on the dechanneling cross section dependence on analyzing beam [2]. The variation of the channeling minimum yield χ_{min} measured directly behind the damage peak as a function of the incident ^{4}He-ion energy is shown in Fig. 8.

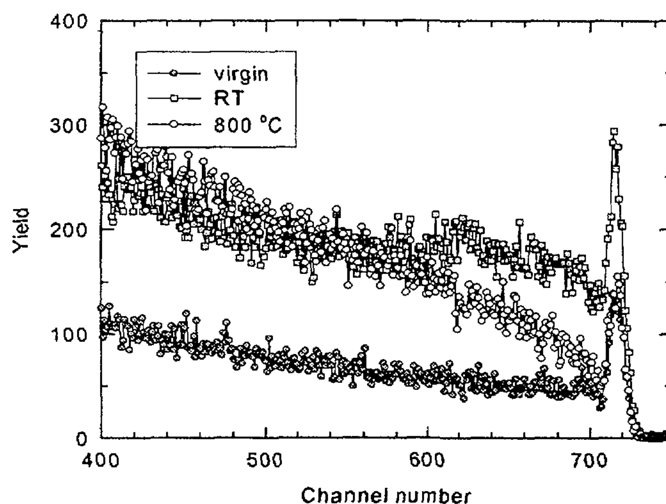

Fig. 7. Aligned spectra for virgin and ion implanted GaN epilayers subjected to Mg-ion implantation at different temperatures.

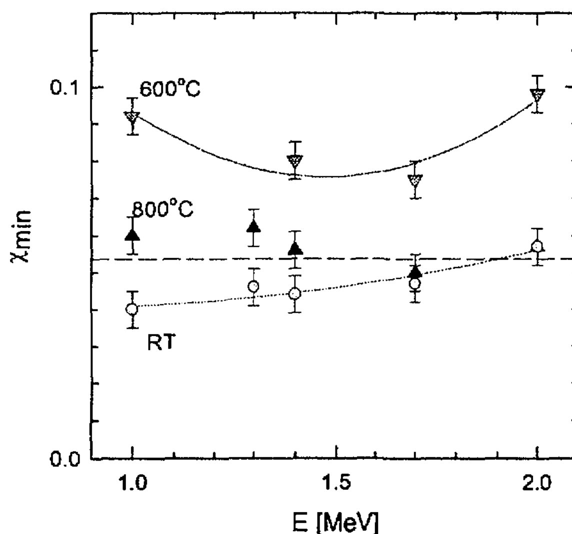

Fig. 8. Results of the energy dependent analysis of GaN epilayers implanted at different temperatures.

3.2. Conclusions

After RT implantation the small defect clusters of different size and morphology were formed. In the implanted region a non-uniform increase of the lattice parameter was observed due a rather large compressive strain produced by defects. The increased defect mobility during ion implantation at 600°C and 700°C resulted in the defect migration to the larger depths and enhanced defect clustering. Important changes were observed after implantation at 800°C. X ray diffraction revealed that defects produced at this temperature are to the high extent coherent with the host lattice. RBS/channeling analysis provided evidence that these defects are predominantly stacking faults.

4. Characterization of InGaN/GaN Heterostructres

4.1. Background

In last years, the InGaN/GaN heterostructures have attracted a great interest because of their application for the production of light emitting devices [9]. The extensive utilization of $In_xGa_{1-x}N$ alloy as the active layer is principally due to the tunability of its energy gap. By changing its composition light spectrum from the red (x=1) to near ultraviolet (x=0) can be covered. In spite of the large efforts, the growth and properties of InGaN have not been completely optimized or understood yet. The difficulty of growing InGaN epitaxial layers on GaN substrates is principally caused by the large difference of lattice constant between these two materials of 11% [10]. It results in the large strain even in the layers of low In-concentrations. At higher In-concentrations two types of structural transformations are observed: phase separation and atomic ordering [11]. The observed phase separation is driven by the strain. To reduce the strain energy of the system In atoms are expelled from the InGaN lattice to form an alloy of different composition.

4.2. Results

InGaN alloy layers were grown by the MOCVD technique at a temperature of 800°C. Before the deposition of InGaN layers, a few μm thick GaN layers were grown on c-plane sapphire at a temperature of 1050°C. The thickness of InGaN layers varied from 30 nm to 110 nm and their composition ranged from x = 0 to x = 0.12.

Samples were characterized using RBS/channeling as the analytical method for the determination of principal properties of epitaxial layers, like: In-content, thickness, crystalline perfection, lattice distortion, and stress. 2 MeV ^{4}He-beam was applied. The detection angle was165° and the energy resolution was 15 keV.

Fig. 9 shows the high-energy portions of random and aligned spectra for the InGaN/GaN heterostructure. The arrows indicate the scattering energy of Ga and In atoms at the surface. For InGaN layers of thickness not exceeding 120 nm the In peak is well separated from the Ga continuous spectrum. Since the height of the In peak is a measure of its content the flat top of the peak confirms the In uniform concentration in the layer. The aligned spectrum taken for a heterostructure of x = 0.03 revealed χ_{min} = 2 % for Ga and χ_{min} = 6 % for In indicating its reasonable crystalline quality as compared to χ_{min} = 2% for Ga in the GaN substrate. The χ_{min} values for both elements increase with the In content as shown in Fig.10. The increase is linear as demonstrated by solid line in Fig.10 fitted to the data by the least square method. It has been observed that such linear dependence holds up to x = 0.30 (not shown in Fig.10). One notes the χ_{min} for Ga is always lower than that for In although the difference between them changes rather accidentally.

In order to study the lattice distortion in the $In_xG_{1-x}aN$ layer with x = 0.09 the angular scans were measured for different axes in the $(1\bar{2}10)$ plane. Fig.11 shows the angular scans measured for the principal [0001] axis and $[10\bar{1}1]$ axis. Three windows were set: (i) — for Ga in the bulk, (ii) — for Ga in the layer, and (iii) for In in the layer. For the [0001] axis all three dips have the same location of their minimum but slightly different critical angles: $\Theta_c = 0.74^\circ$ for Ga in the bulk and $\Theta_c = 0.80^\circ$ for Ga and In in the epilayer. Completely different behaviors exhibit the dips for the $[10\bar{1}1]$ axis. Both layer dips are significantly shallower but the In and Ga dips are shifted towards lower angles with respect to the bulk Ga dip. The negative value of $\Delta\Psi = \Psi_{epi}-\Psi_{bulk}= -0.35^\circ$ indicates the tetragonal distortion of the InGaN layer due to the tensile stress in the perpendicular direction.

The c/a ratio amounts to $\sqrt{3}/\tan\Psi_{epi} = 1.670$. Powell et al. [12] showed that for GaN epitaxial layer on sapphire $a_b = 0.3185$ nm. Assuming that the InGaN layer has not relaxed, i.e. $a_{epi} = a_b$, c amounts to 0.5244 nm. In order to calculate perpendicular $\epsilon^{\perp} = (c_{epi}-c_b)/c_b$ and parallel $\epsilon^{\parallel} = (a_{epi}-a_b)/a_b$ strains in the layer lattice constants of relaxed $In_xGa_{1-x}N$ are necessary. The data for InN were taken from Paszkowicz [13] and $c_b = 0.52039$ nm and $a_b = 0.31994$ nm for x = 0.09 were calculated using Vegard's law. The deduced values are: perpendicular strain $\epsilon^{\perp} = 0.77\%$, and parallel strain $\epsilon^{\parallel} = -0.45\%$. These parameters indicate that the layer is under tensile stress in the perpendicular direction and under the compressive stress in the parallel one.

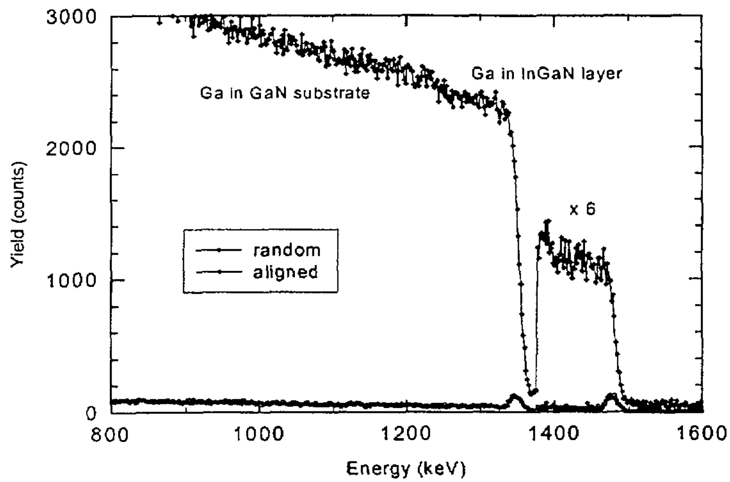

Fig. 9. Random and aligned spectra for InGaN/GaN heterostructure.

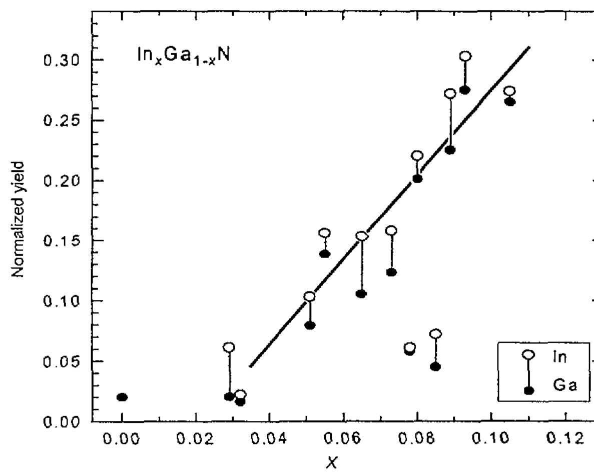

Fig. 10. Minimum channeling yields for In and Ga in the $In_xGa_{1-x}N$ epilayer as a function of x.

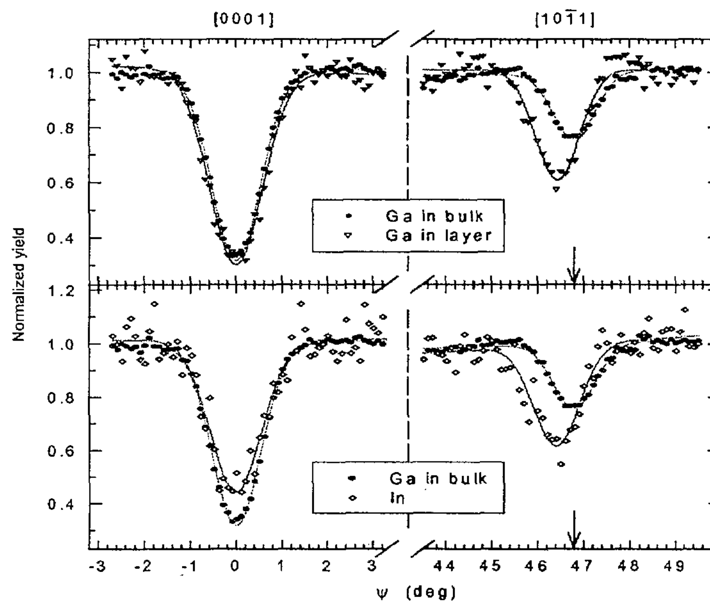

Fig. 11. Angular dips measured along the (1$\bar{2}$10) plane for two different axes. The dips obtained for the bulk Ga were compared with dips measured for the epilayer for: In (a) and (b), and Ga (c) and (d), respectively.

4.3. *Conclusions*

The great advantage of RBS/channeling when applied to analysis of $In_xG_{1-x}aN$ layers with 0<x<0.15 can be produced by MOCVD technique on GaN/sapphire is that it allows determination of variety of parameters. These are:

- In content in strained layers can be directly measured,
- magnitudes of tetragonal distortion and strain can be determined by measurement of angular scans across principal, i.e. normal to the surface axis and one of the other axes with low crystallographic indices,
- crystalline quality can be deduced from aligned spectra.

The last observation revealed continuous increase of χ_{min} with x indicating In precipitation. Apparently raising stress caused by In oversaturation is a driving force for phase segregation. This hypothesis is also confirmed by the split of PL spectrum into two peaks as observed in some samples. It is generally accepted that phase segregation leads to the relaxation of strained epilayers, however, the value of 3.4 eV of PL peak energy for x = 0 [14] and channeling angular scans clearly indicate that the layers are still strained.

5. Monte Carlo Simulation of Channeling Spectra

Evaluation of channeling data measured at different temperatures requires consideration of several usually neglected factors. First of all, changes of thermal vibration amplitudes of crystal atoms have to be taken into account. Moreover, the III-N semiconductor compounds are rather sensitive to the He-ion bombardment, especially at low temperatures. Thus, the production of defects by the analyzing beam and their partial annealing upon warming up cannot be neglected. With this respect only the Monte Carlo simulations of channeling spectra can be successfully applied. Such simulations were performed using the computer code developed at SINS Warsaw. For calculations the crystal is divided into "slices" each of them containing one atomic plane. The particle trajectory is calculated as a binary collision with each sequential atom. Thermal vibrations of atoms are also included by randomly changing their position around the regular lattice positions. Moreover, the stopping power of channeled beam is impact parameter dependent and is calculated according to the modified Lindhard approximation [15]:

$$\varepsilon_{ch} = (1-\alpha)\,\varepsilon_R + \alpha\,\varepsilon_R\, n_e(r)/n_e$$

where: ε_R stopping cross section for random direction, $n_e(r)$ and n_e are local and average electron density. For perfectly channeled particles α=0.5 whereas for the random direction α=0.

The amplitudes of thermal vibrations for 300 K and 21 K were determined by fitting the aligned spectra shown in Fig.12 with our Monte Carlo simulation code. The thermal vibration amplitudes were considered equal for each component specie and amounted to u_{21K} = 5.0 pm and u_{RT} = 6.7 pm. These amplitudes were then used in simulations of implanted crystals.

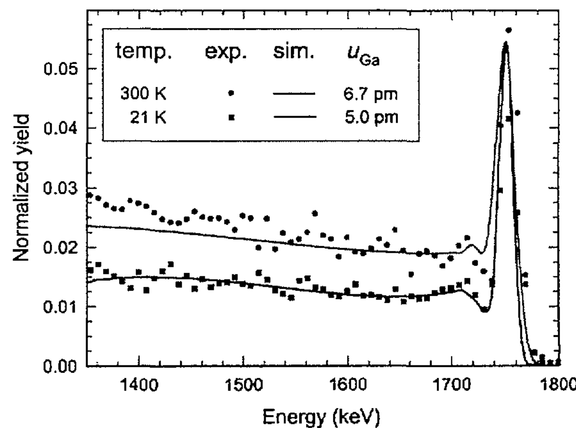

Fig. 12. Aligned spectra taken for the same GaN single crystal at two different temperatures.

Selfinterstitial atoms, vacancies and antisites are considered as simple defects in compound crystals. The contribution of the two last defects to the dechanneling yield is usually negligible. Since in this case σ_D can be calculated analytically [2] it seems that it would be the easiest task for the channeling analysis. However, the problems arise if the defect content is so high that a part of the aligned spectrum is close to the random one. The possible defect clustering and increasing influence of multiple scattering can make such an analysis unreliable.

A typical example of this kind analysis is illustrated in Fig. 13. The first MC calculations were performed using $\alpha = 0$ and somewhat surprisingly they fitted the experimental spectrum very well. Since the aligned spectrum exhibits very low damage level in the near surface region (1650–1450 keV) the use of α close to 0.5 seemed to be more appropriate. In spite of this presumption the spectrum calculated with $\alpha = 0.5$ is shifted to lower energies well behind the damage peak. The depth distribution calculated with $\alpha = 0$ fits well the defect distribution calculated with the TRIM code whereas that with $\alpha = 0.5$ is located significantly deeper. In addition, the defect distribution calculated using the two-beam approximation method (TBA) coincides well with that of TRIM. In order to check whether the TRIM estimates are correct the projected range of implanted hydrogen was measured using NRA. Accidentally the implanted H distribution almost overlaps with the MC defect profile calculated with $\alpha = 0.5$. Consequently, the real defect profile must be located at shallower depth.

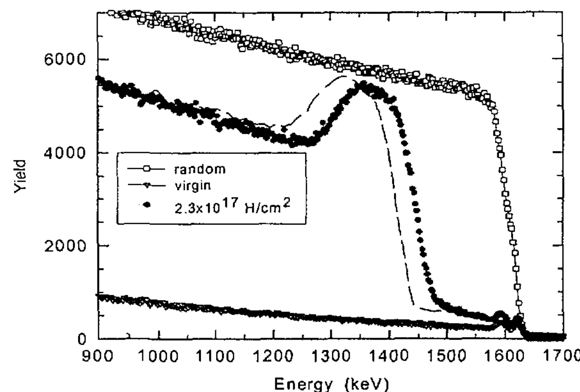

Fig. 13. Random and aligned spectra for GaAs single crystal implanted with 2.3 × 10^{17} H/cm^2. The solid lines show the result of Monte Carlo simulations with $\alpha = 0$. The spectrum calculated with $\alpha = 0.5$ is shown by dotted line.

5.1. Conclusions

The Monte Carlo method for channeling spectra simulations enables not only detailed analysis of the perfection of the crystalline structure of analyzed samples but also can provide information on physical parameters difficult or even impossible to obtain using other experimental methods. This especially concerns the amplitudes of thermal vibration of lattice atoms. Monte Carlo evaluation of channeling spectra taken at different temperatures can be used for determination of such amplitudes and consequently of Debye temperature.

6. Hydrogen Implantation in GaAs

6.1. Background

The performance of semiconductor micro- and optoelectronic devices can be greatly enhanced if one can freely integrate different materials. An effective integration method has remained a challenge due to lattice constant mismatch between semiconductor systems. Heteroepitaxial growth of highly mismatched materials can result in layers containing large concentrations of defects, which degrade or inhibit device operation. Because of this limit of heteroepitaxial growth, a variety of methods of material joining techniques have been developed over the last decade [16]. One of the most elegant methods is direct wafer bonding technology. Bonding by Van der Waals forces occurs when two clean and smooth surfaces are placed in contact.

6.2. Results

Hydrogen ion implantation in (100) GaAs single crystals was performed at ITME Warsaw at temperatures ranging from 45°C to 160°C. Implantation energy was 50 keV and the doses ranged from 4×10^{16} H/cm^2 to 4×10^{17} H/cm^2. Depth distribution of hydrogen was measured using the $^{15}N(p,\alpha\gamma)^{12}C$ nuclear reaction at SUNY Albany, whereas, the 2 MeV ^{4}He-ion channeling was applied for defect analysis at SINS Warsaw. Surface morphology after hydrogen bombardment and thermal treatment leading to the surface layer exfoliation was studied by means of SEM (scanning electron microscopy) and optical microscopy. Surface roughness was determined by the Alphastep profilometer in terms of the roughness parameter Ra, i.e. the mean arithmetic value of the surface irregularities. Surface blistering occurs if the ion dose exceeds a given critical value, which in turn depends on the target temperature during implantation.

As shown in Fig.14, no surface defects induced by ion implantation at temperatures below 100°C were observed up to a highest used ion dose of 4×10^{17} H/cm^2. Blistering and flaking occur upon ion implantation at temperatures exceeding 100°C at ion doses already less than 1×10^{17} H/cm^2. The measured critical ion dose amounted to 9×10^{16} H/cm^2 at 140°C and decreased to 7×10^{16} H/cm^2 at 160°C. The increase of the ion dose over the critical value at a given temperature results in the increase of the amount of blisters and their dimensions. Variation of the surface roughness parameter, Ra, with the ion dose is shown in the inset in Fig.14. One notes that blisters grow more rapidly at higher temperatures.

Structural defect formation and transformation was studied by means of RBS/channeling. Fig. 15 shows spectra for H implantation at 45°C (curves 2,3,6) and at 140°C (curves 4,5). As can be seen, hydrogen implantation at 45°C produces damage peaks that increase with the increase of the ion dose. In all cases, even for the heavily damaged crystal implanted with 2.3×10^{17} H/cm^2 only simple defects and/or small amorphous clusters were detected [17]. This is in agreement with the observation that no detectable blisters or other forms of surface deformation were observed after low temperature hydrogen implantation up to the fluence of 4.0×10^{17} H/cm^2. Surprisingly, the damage peak for samples implanted at 140°C was significantly greater than that for samples implanted with the same dose at a lower temperature (cf. curves 2 and 3, and curves 4 and 5 in Fig. 15). One could expect the opposite effect because of the increased defect mobility at elevated temperatures leading to the enhanced defect recombination probability.

Results of the NRA analysis are shown in Fig.16. The concentration profile of hydrogen implanted with a dose of 6×10^{16} H/cm^2 was obviously not influenced by the implantation temperature (120°C) and post implantation annealing up to 300°C. Additionally, similar results were obtained for implantation carried out at 200°C or post implantation annealing at 400°C. Taking into account very good depth resolution of the NRA (approx. 10 nm) only short-range rearrangement of hydrogen atoms can occur at temperatures below 400°C.

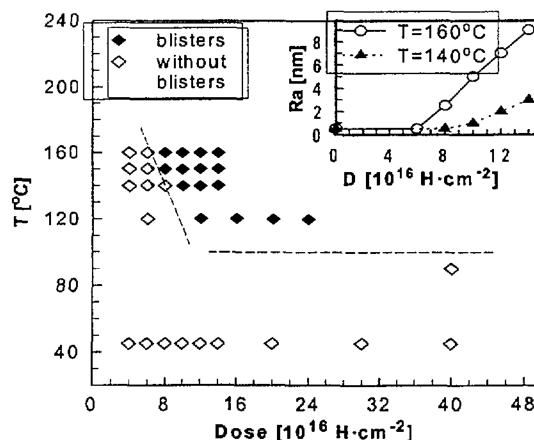

Fig. 14. Dose and temperature boundaries of blister formation in hydrogen implanted GaAs. The inset shows the roughness parameter dependence on the implanted hydrogen dose.

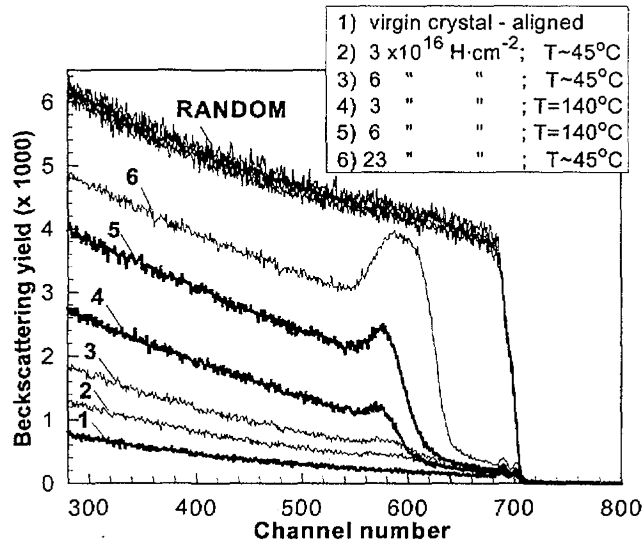

Fig. 15. Random and aligned RBS spectra for GaAs single crystals implanted with various hydrogen doses at two different temperatures.

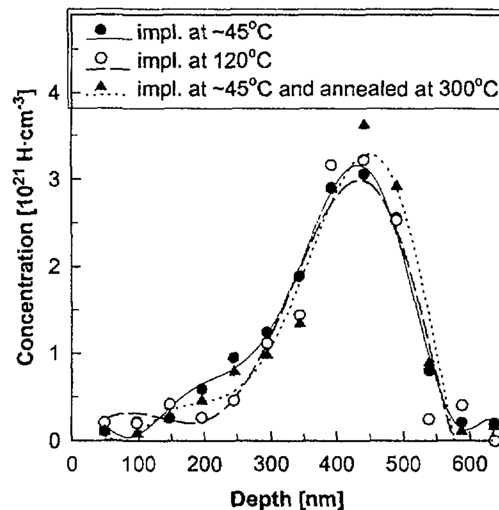

Fig. 16. Hydrogen concentration profiles for GaAs single crystals implanted with 6 × 10^{16}H/cm^2 at different temperatures as determined by the NRA analysis.

6.3. Conclusions

In the first part of the reported experiments, the conditions for blisters formation were investigated. Blistering is directly responsible for the formation of microcracks which in turn produce layer splitting. No blistering was observed at temperatures below 100°C even after implantation with a dose as large as 4 × 10^{17} H/cm^2. In order to provoke blistering in such samples an annealing at temperatures exceeding 400°C is necessary [18]. Blistering is much more easily obtained upon hot implantation. There are two distinct temperature regions: at temperatures below 90°C no blisters were found, whereas, at temperatures exceeding 120°C appreciably high blister density can be observed. In the second range the temperature at which blistering occurs depends on the implantation dose. The growth of blister dimensions with increasing implantation temperature is reflected in the rapid increase of surface roughness.

The complementary investigations of defect behavior and hydrogen depth distributions gave some insight into the mechanism of blister formation. The important conclusion from the NRA

analysis is that the hydrogen concentration profile is altered neither upon hot implantation nor upon annealing at temperatures at least not exceeding 300°C. Thus, at these conditions, the distance of hydrogen atom migration most probably does not exceed a few nanometers. According to Rauhala and Räisänen [18] the maximum damage distribution is located at the same depth as that of the hydrogen atom distribution. This was confirmed by our RBS/channeling measurements. Moreover, the detailed study of the damage structure [19] revealed that after RT implantation only displaced atoms and/or small amorphous clusters are formed. The substantial increase of the damage peak after hydrogen implantation at temperatures above 140°C as compared to that measured for the sample implanted with the same dose at 45°C is somewhat unusual. One could expect the opposite effect, i.e. a decrease of the damage peak due to greater defect mobility. It is worth pointing out that at this temperature only defects in the Ga sublattice are mobile in GaAs, whereas, defect mobility threshold for As sublattice lies above 300°C [20]. Thus, important defect transformations cannot be expected in the studied temperature range. Furthermore, the study of hydrogen diffusion in GaAs [21] clearly indicated that hydrogen mobility is largely suppressed by the presence of radiation damage. All these factors lead to the conclusion that the unusual increase of damage peaks in channeling spectra for samples implanted at 140°C is due to the formation of hydrogen-defect complexes in which matrix atoms become displaced from their lattice sites. One notes, that according to the data shown in Fig.14 at the applied doses no blisters are formed. Since gas bubbles and voids have relatively low dechanneling cross-sections such defects cannot be the dominant kind of defect. Therefore, the observed hydrogen-defect complexes of different morphology containing multiple hydrogen atoms bounded to displaced matrix atoms can be considered as precursors of the hydrogen bubble and eventually blister formation. They are effective traps for mobile hydrogen atoms and stabilize the radiation damage produced by ion implantation. The prerequisite of such complex formation is high enough hydrogen concentration. Their formation is thermally activated: small complexes can only coalesce if the implantation temperature exceeds 120°C or after annealing at temperatures above 400°C.

6.4. Hydrogen Content Analysis in GaN

GaN single crystals and epilayers are usually produced as a n-type. This is apparently due to the easy formation of N vacancies during the growth. The p-type GaN, which is necessary for the formation of p-n junctions, is difficult to obtain. This is most probably due to the incorporation of large quantities of hydrogen atoms already during the growth process. Hydrogen is known to passivate the p dopants leading to reduction of their electrical activity. Hydrogen content in GaN was measured by means the ERD (M.Budnar) and the NRA (W.Lanford and FZ Rossendorf) techniques. The obtained results can be summarized as follows:

- single crystals contain in the average less than 0.1 at% of H, which is below the detection limit of both methods,
- thin foils and sintered powders contained between 0.5 to 5 at% of H depending on the growth conditions, however, no direct correlation was observed,
- extensive H outdiffusion was observed at the beginning of the analysis indicating release of hydrogen atoms from the outermost layers. After this initial period the reaction yield has stabilized.

REFERENCES

[1] DOOLITTLE, L.R.,Nucl.Instr. and Meth. **B9** (1985), 344.

[2] FELDMAN, L.C., MEYER, J.W., PICRAUX, S.T., Materials Analysis by Ion Channeling (Academic Press, New York, 1982).

[3] ZIEGLER, J.F.,.BIERSACK, J.P, LITTMARK, U. The stopping and Range of Ions in Solids, vol.1 (Pergamon Press, New York, 1985).

[4] Kabayashi, H., Gibson, W. M., Appl. Phys. Lett. **73** (1998) 1406.

[5] LIMMER, W., RITTER, W., SAUER, R., MENSCHING, B., LIU, C., RAUSCHENBACH B., Appl. Phys. Lett. **72** (1998) 2589.

[6] LIU, C., MENSCHING, B., ZEITLER, M., VOLZ, K., RAUSCHENBACH, B., Phys. Rev. **B57** (1998) 2530.
[7] MIYACHI, M., TANAKA, T., KIMURA, Y., OTA H., Appl. Phys. Lett. **72** (1998) 1101.
[8] PONG , B.J., PAN, C.J., TENG, Y.C., CHI, G.C., LI, W.-H., LEE, K.C., J. Appl. Phys. **83** (1998) 5992.
[9] NAKAMURA, S., SENOH, M., NAGAHAMA, S., IWASA, N., YAMADA, T., MATSUSHITA, T., KIYOKU, H., SUGIMOTO, Y., KOZAKI, T., UMEMOTO, H., SANO, M., CHOCHO, K., Appl.Phys.Lett., **72** (1998) 211.
[10] MATSUOKA, T., SASAKI, T., KATSUI, A., Optoelectron., **5** (1990) 53.
[11] DOPPALAPUDI, D., BASU, S.N., LUDWIG, K.F., MOUSTAKAS, D., J.Appl.Phys., **84**(1998)1389.
[12] POWELL, R.C., LEE, N.-E., KIM, Y.-W., GREENE, J.E., J.Appl.Phys., **73** (1993) 189.
[13] PASZKOWICZ, W., Phil.Mag. **A 79** (1998) 1145.
[14] MCCLUSKEY, M.D., VAN DE WALLE, C.G., MASTER, C.P., ROMANO, L.T., JOHNSON, N.M., Appl.Phys.Lett., **73** (1998) 2725.
[15] LINDHARD, J, J.Mat.Fys.Medd.Dan.Vid.Selsk. **34** (1965) nr.14.
[16] BRUEL, M., Electronics Lett. **31** (1995) 1201–1202.
[17] JALGUEIER, E., ASPAR, B., POCAS, S., MICHAUD, J. F., ZUSSY, M., PAPON, A. M., BRUEL, M., Electronics Lett. **34** (1998) 408–409.
[18] RAUHALA, E., RÄISÄNEN, J., Nucl.Instr. and Meth. **B94** (1994) 245–250.
[19] STONERT, A., TUROS, A., NOWICKI, L., BREEGER, B., Nucl.Instr. and Meth. **B161-163** (2000) 496–500.
[20] TUROS, A., STONERT, A., BREEGER, B., WENDLER, E., WESCH, W., FROMKNECHT, R., Nucl.Instr.and Meth. **B148** (1999) 401–405.
[21] RÄISÄNEN, J., KEINONEN, J., KARTTUNEN, V., KOPONEN, I., J.Appl. Phys. **64** (1998) 2334–2336.